

Received September 3, 2019, accepted October 3, 2019, date of publication October 15, 2019, date of current version October 30, 2019.

Digital Object Identifier 10.1109/ACCESS.2019.2947481

Cross-Configuration Substrate Integrated Waveguide Beamforming Network for 1D and 2D Beam Patterns

CHAD BARTLETT AND JENS BORNEMANN¹, (Fellow, IEEE)

Department of Electrical and Computer Engineering, University of Victoria, Victoria, BC V8W 2Y2, Canada

Corresponding author: Jens Bornemann (j.bornemann@ieec.org)

This work was supported by the Natural Sciences and Engineering Research Council (NSERC) of Canada.

ABSTRACT This paper presents the simulated and measured results of a dual-layer substrate integrated waveguide (SIW) beamforming network utilizing an 8×8 cross-configuration Butler matrix over a frequency range of 28.5 to 31.5 GHz. By arranging the input ports on the bottom SIW layer and employing dual-layer passband filters as a detachment point, the top SIW layer can be interchanged with the purpose of exploring one-dimensional and two-dimensional broadside beam patterns. Although Butler matrices are not typically utilized for beamforming in this configuration, two examples of interchangeable top layer arrays are demonstrated; the first being a 2×8 slot antenna array for 1-D scanning, and the second being a 2×4 center-slot array for 2-D scanning. Each of the beamforming network's simulated and measured 10 dB bandwidth is demonstrated over a range of 28.5 to 31.5 GHz. Additional design details and dimensions are specified for the aforementioned passband filter transitions, as well as for each of the slot antenna arrays.

INDEX TERMS Butler matrix, millimeter-wave, slot antenna array, substrate integrated waveguide (SIW), dual-layer SIW filters.

I. INTRODUCTION

An ever-increasing demand for wider bandwidths in communication, radar, and imaging systems has emerged. In order to facilitate this growing demand, progressive research into millimeter-wave technologies has become vital in achieving next generation networks such as 5G. Being cost effective and easy to manufacture, substrate integrated waveguide (SIW) circuits have been demonstrated as a viable candidate for high-frequency applications due to their low-loss, high quality-factor, and high power-handling capabilities [1]–[3].

Research on beamforming networks (BFNs), specifically the Butler matrix, has demonstrated powerful beam-steering capabilities through the use of passive component networks. Work in [4]–[16] – and many others – have been able to demonstrate successive advancements with SIW BFNs for one-dimensional and two-dimensional beam patterns. Through these clever configurations, cost effective and robust options are available for us to use.

The associate editor coordinating the review of this manuscript and approving it for publication was Guan-Long Huang².

In order to further millimeter-wave research in this area, this paper presents a modified configuration of the Butler matrix in SIW with the following new aspects:

First, to the best of the authors' knowledge, this is the first 8×8 cross-configuration Butler matrix in SIW technology; secondly, the system incorporates bandpass filtering capabilities which significantly reduces the need for additional filtering functions within the RF chain; thirdly, the system is physically reconfigurable by separation of the Butler matrix from the antenna array at a pre-selected point (the filters). This allows for the array to be easily interchanged with other one-dimensional, and two-dimensional slot antenna arrays for additional beam width and direction options.

Note that although the last aspect does not fall under the rigorous definitions of reconfigurable antennas, the interchangeability of 1-D and 2-D arrays is considered an added benefit that is not typically expressed in Butler matrix configurations.

The design and simulations are carried out in CST Microwave Studio in order to inspect system characteristics. Component design techniques for similar hybrid couplers, cross-couplers, and phase shifters can be reviewed in the

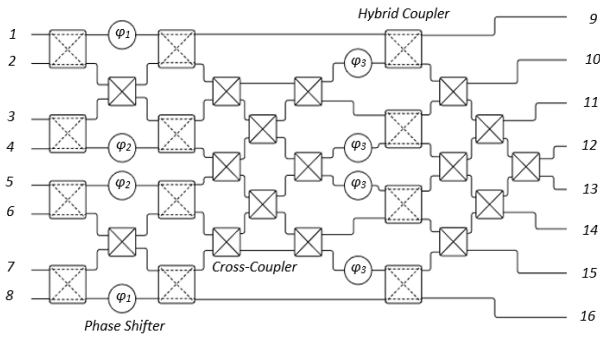


FIGURE 1. Ideal 8 × 8 Butler matrix.

literature [15]–[17]. Circuit prototypes are manufactured and tested to validate simulation results. The dual layer SIW is fabricated on Rogers Duroid 5880 substrate with a thickness of 0.508 mm, and a dielectric constant of $\epsilon_r = 2.2$. The metalized via spacing, a_{SIW} , for the SIW walls is calculated to be 5.0 mm using (1) from [18], where the diameter d of the vias is set to be 0.3 mm, the spacing p is 0.56 mm, and the effective waveguide width W_{equi} is found from (2)

$$a_{SIW} = W_{equi} + p \left(0.766e^{0.4482d/p} - 1.176e^{-1.214d/p} \right) \quad (1)$$

$$W_{equi} = \frac{c}{2f_c \sqrt{\epsilon_r}} \quad (2)$$

where c is the speed of light and f_c the cutoff frequency.

II. ANTENNA FEED-NETWORK LAYER

The beamforming network is in the arrangement of a 8 × 8 Butler matrix [19]. Fig. 1 depicts the ideal layout of the Butler matrix. Phase shifters $\varphi_1 - \varphi_3$ correspond to -67.5° , -22.5° , and $+45^\circ$, respectively. The input ports are labeled 1 through 8, while the output ports are labeled 9 through 16. By exciting one of the input ports, the Butler matrix divides the signal equally between each of the output ports. The relative phase difference – or phase progressions – between each of the output ports will be determined by which input port is selected for excitation. For input ports 1 through 8, the phase progressions between sequential outputs will correspond to either $\pm 22.5^\circ$, $\pm 67.5^\circ$, $\pm 112.5^\circ$, or $\pm 157.5^\circ$. Fig. 2 depicts the rearrangement of the equivalent Butler matrix into a planar cross-configuration [20], [21]. Upon comparing Fig. 1 and Fig. 2, it can be noted that the number of cross-over couplers has been reduced from 16 to 6, while the number of hybrid couplers and phase shifters remain the same.

By converting the circuit into SIW technology (proceeded in Fig. 3 and Fig. 4 (a)), further rearrangement can take place. First, it must be noted that the cross-over couplers and additional 90° corner feed-line lengths both contribute non-negligible phase differences. Phase compensation can be taken into account by developing φ_1 and φ_2 with respect to their adjacent cross-over couplers. Next, the longest feed path of an input port to an output port should be observed. By doing so, the circuit’s phase distribution can be tuned more

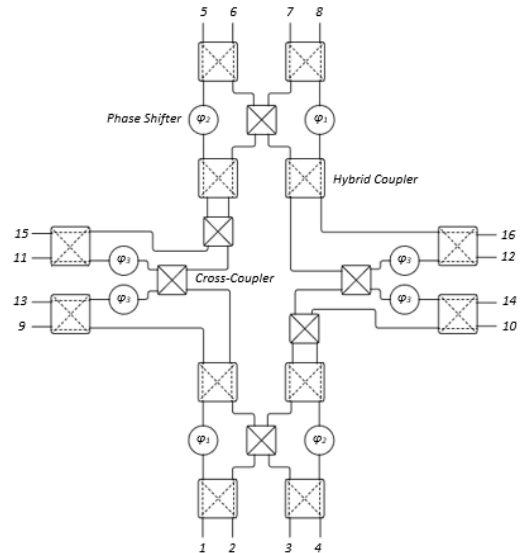


FIGURE 2. Equivalent 8 × 8 cross-configuration Butler matrix.

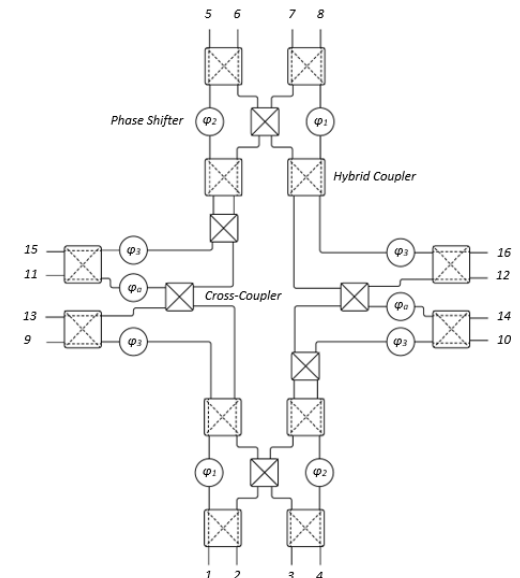


FIGURE 3. 8 × 8 cross-configuration Butler matrix with compensating phase shifters.

easily. For example, when comparing the circuit paths from port 1 to each of output ports 9 through 16, it can be determined that the path between port 1 and port 16 has the longest electrical length. To achieve the proper operation of the Butler matrix, the next sequential port (15) requires a 22.5° phase difference. In this manner, φ_a is introduced as a 0° phase shifter to compensate for the second cross-over coupler in the port 1 to port 16 path. By doing so, the desired phase relation between ports 15 and 16 is obtained. Following this pattern, the circuit is adjusted to achieve the proper phase relations between each of the sequential outputs. Fig. 3 depicts the final matrix scheme while Fig. 4 (a) depicts the via hole layout in SIW. In Fig. 3, elements φ_3 become -45° phase shifters, while in Fig. 4 (a) they can be tuned to ensure the proper

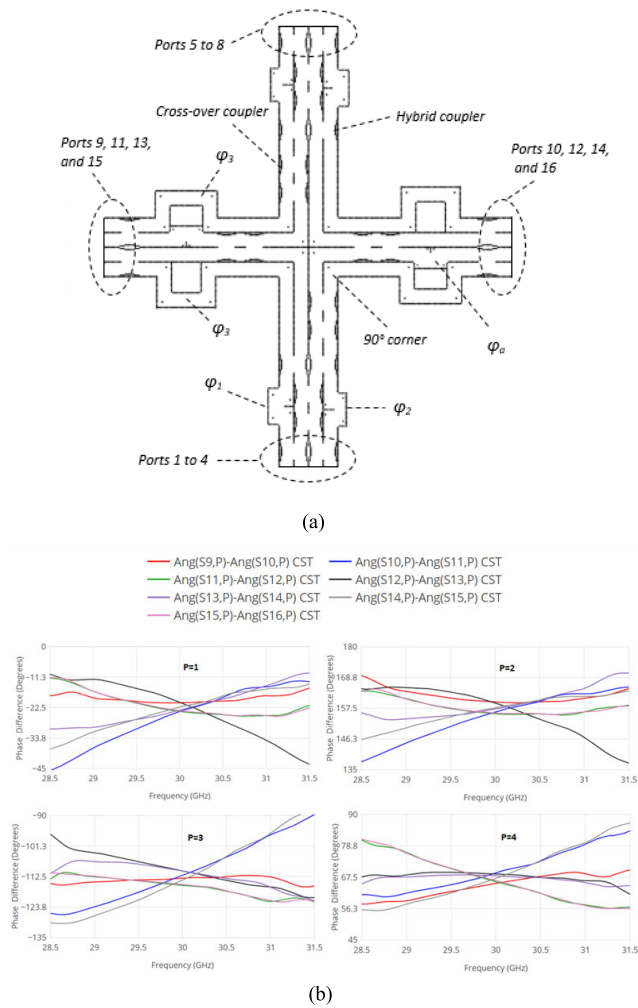


FIGURE 4. (a) 8×8 cross-configuration Butler matrix in SIW and (b) the output phase progressions for ports 1 through 4.

phase relations between output ports. Fig. 4 (b) illustrates the phase progressions developed at the outputs of Fig. 4 (a) when ports 1 through 4 are excited.

Now in a cross-configuration, ports 9 through 16 are separated by a large spacing – far greater than an optimal spacing of $\lambda/2$ – and no longer situated in sequential (or inline) order. The attachment of antennas at these points would generally cause large grating lobes and beamforming problems. By incorporating folded dual-layer direct-coupled passband filters, a second SIW layer can be attached at ports 9 through 16 in order to transfer the power – as well as maintain the necessary phase shifts – to a more functional array with optimal λ spacing. By maintaining the input ports 1 through 8 on the bottom SIW layer, the folded dual-layer filters can also serve as a detachment point for interchangeable array configurations that are fabricated into new top SIW layers (c.f. Section III). Fig. 5 depicts the center view of a dual-layer filter.

Fig. 6 depicts the properties of the 26 to 34 GHz filter. In this manner, the filters encompass the Butler matrices

TABLE 1. Dual-layer filter dimensions (mm).

S_f	W_f	W_{Af}	D_f	D_{Af}	D_{IA}
0.86	2.00	1.65	3.18	3.19	0.30

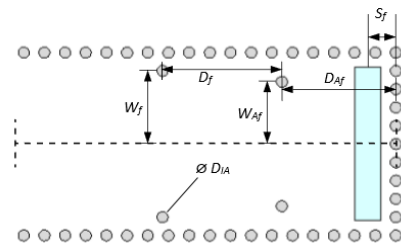


FIGURE 5. Direct coupled dual-layer SIW passband filter geometries.

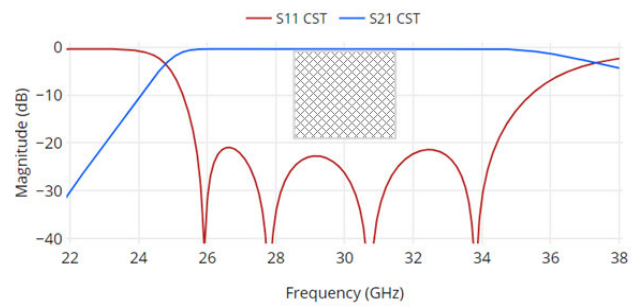


FIGURE 6. Simulated dual-layer SIW passband filter S-parameters.

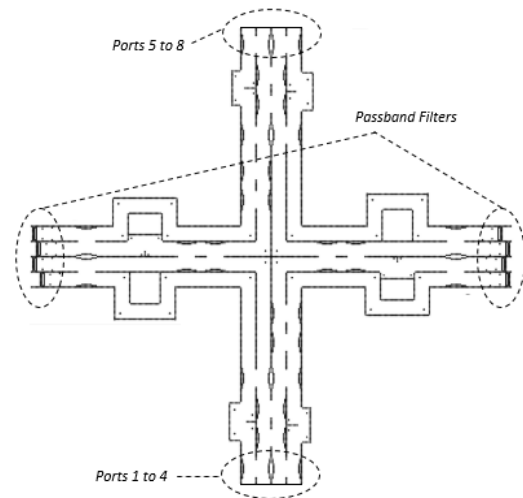


FIGURE 7. Bottom SIW layer; Butler matrix and passband filters shown.

frequencies of interest (the cross-hatched inset). Although the filter bounds are set wide for this example, more dramatic effects such as transmission zeros can be added for specific applications. Fig. 5 and Table 1 detail the design dimensions of the filter structure. The slot is 0.7 mm \times 4.1 mm. The bottom SIW layer containing the Butler matrix feed-network and bottom-half portions of the dual-layer filters is shown in Fig. 7.

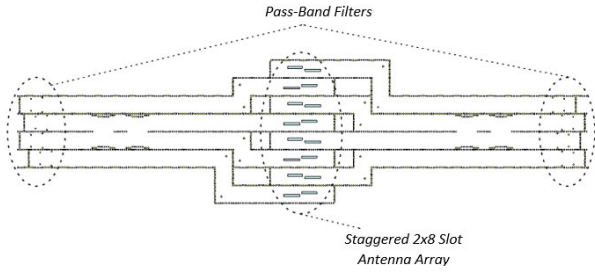


FIGURE 8. Top SIW layer with 2 × 8 slot antenna array.

TABLE 2. 2 × 8 slot antenna dimensions (mm).

S_1	W_1	W_{A1}	L_1	L_{A1}	D_1
7.01	0.325	0.375	4.40	4.20	4.90

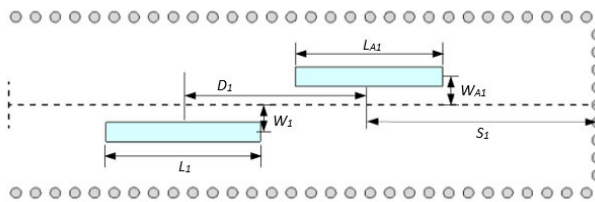


FIGURE 9. Geometries of the slot antennas for the 2 × 8 array.

III. ANTENNA ARRAY LAYERS

A. 1-D SCANNING ARRAY

For the design of the top-layer 1-D scanning antenna array, resonant slot antennas are selected to form a 2 × 8 array. Due to the antenna array being fed from both ends of the bottom-layer Butler matrix, signal path rearrangement is required once more for the proper phase distribution of signals. This redistribution is achieved by the use of two additional cross-over couplers in the top layer. Fig. 8 depicts the top SIW layer for the 1-D scanning array. Additionally, staggering of the dual-layer filter positions – as seen in Fig. 7 and Fig. 8 – is meant to offset the feed path lengths and crossover couplers that feed the antennas in the top layer. Fig. 9 and Table 2 demonstrate the antenna dimensions for the 2 × 8 array; slot widths are 0.55 mm. Spacing between the antenna structures is $\lambda/2$. The S-parameters of port 1 are shown in Fig. 10 and demonstrate a reflection coefficient and isolation better than 10 dB over the 28.5 – 31.5 GHz range for the 2 × 8 antenna array; analyses of the other ports provide similar results.

Fig. 11 illustrates the mounting of the 1-D antenna array to the bottom-layer feed network. This 1-D array structure allows for horizontal beam maxima at approximately $\pm 7.0^\circ$, $\pm 22.0^\circ$, $\pm 38.0^\circ$, and $\pm 60.0^\circ$ at 30 GHz. Fig. 12 illustrates the output beam patterns of the system at 30 GHz. The asymmetries depicted are a product of the staggered 2 × 8 slot antenna arrangement in Fig. 8; the most noticeable asymmetries being in the side-lobe levels.

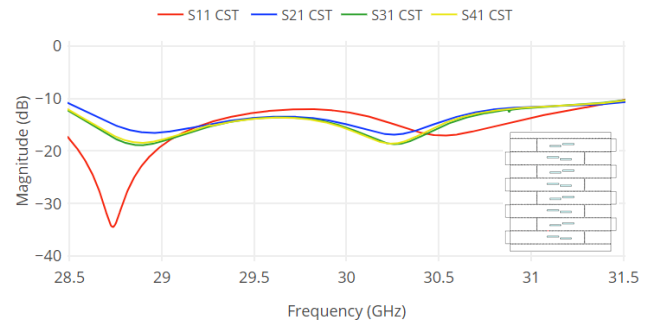


FIGURE 10. Simulated reflection and isolation of the 2 × 8 staggered slot antenna array. Inset depicts the simulated structure.

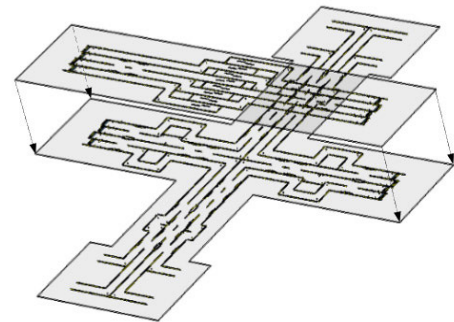


FIGURE 11. Assembly view of the 1-D array and 8 × 8 beamforming network (metallization layers not shown).

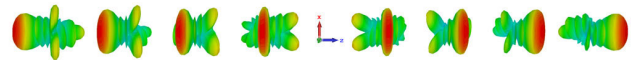


FIGURE 12. Beam patterns of the 1-dimensional array at 30 GHz.

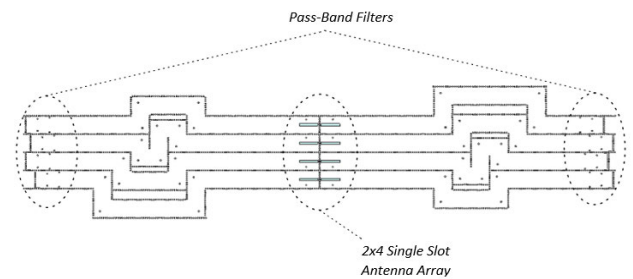


FIGURE 13. Top SIW layer with 2 × 4 center-slot antenna array.

B. 2-D SCANNING ARRAY

For the design of the 2-D scanning antenna array, a 2 × 4 center-slot antenna array was selected. For this second top-layer array, additional cross-over couplers are not required for signal distribution. Similar to the 1-D array, staggering of the dual-layer filter positions is meant to complement the bottom-layer design while fixed phase shifters are arranged to pass the signals with proper phase distribution. Fig. 13 depicts the top SIW layer for the 2-D scanning array. Fig. 14 and Table 3 demonstrate the antenna dimensions for the center-slot 2 × 4 array; slot widths are 0.65 mm.

TABLE 3. 2×4 center-slot antenna dimensions (mm).

S_2	L_2	D_2	D_{A2}	D_{IA2}
2.90	5.10	1.00	3.56	0.30

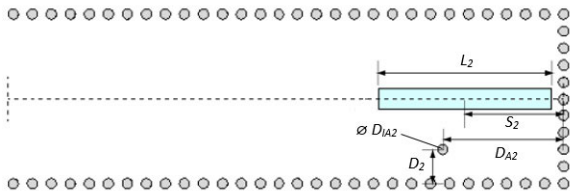


FIGURE 14. Geometries of the center-slot antenna for the 2×4 array.

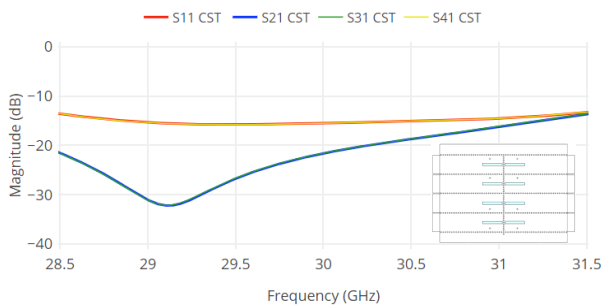


FIGURE 15. Simulated isolation and reflection of the 2×4 center-slot antenna array. Inset depicts the simulated structure.

Spacing between the antenna structures is $\lambda/2$. The S-parameters of port 1 shown in Fig. 15 demonstrate a reflection coefficient and isolation better than -10 dB over the 28.5 – 31.5 GHz range for the 2×4 antenna array; due to a symmetrical layout, analyses of the other ports provide similar results.

The 2-dimensional array structure depicted in Fig. 16 allows for beam maxima coordinates (azimuth, elevation) at approximately $(\pm 10.0^\circ, \pm 14.0^\circ)$, $(\pm 10.0^\circ, \mp 24.0^\circ)$, $(\pm 36.0^\circ, \mp 8.0^\circ)$ and $(\pm 44.0^\circ, \pm 32.0^\circ)$ for 30 GHz. Although the basic operation of the 2-D system is governed by the phase relation developed in the bottom-layer Butler matrix – and then distributed in the top layer – it is important to note that the resulting 2-D beam patterns are also a product of feeding each of the 2×4 array antennas in a juxtaposed (non-sequential) fashion. This arrangement is a direct result of eliminating two of the cross-over couplers from the system. In this manner, the accumulative effect of the diffraction patterns will result in the atypical multi-dimensional beam patterns demonstrated.

Fig. 17 illustrates the output beam patterns of the system at 30 GHz. Note that the pattern asymmetries observed in the 1-D case are not present in the 2-D case due to the symmetry of the antenna layout. However, these beam angles are cross-diagonal symmetric due to the relative phase progressions at the array.

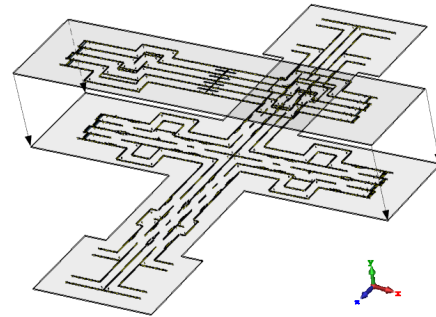


FIGURE 16. Assembly view of the 2-D array and 8×8 beamforming network (metallization layers not shown).

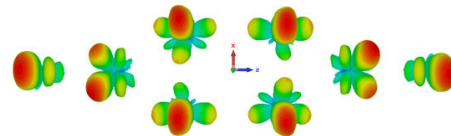


FIGURE 17. Beam patterns of the 2-dimensional array at 30 GHz.

C. COMPARISON

Although the top-layer of the 1-D and 2-D structures differ in design, the feed-paths of both structures – in combination with the staggering of the passband filters – are arranged to help pass the proper phase progressions to their respective antenna arrays. The underlying difference to note is that the location of the sequential output ports is different due to the elimination of two cross-over couplers in the 2-D structure. Interchanging of the top-layer arrays is achieved by physical means. Fig. 11 and Fig. 16 illustrate the mounting of each antenna array layer to the bottom-layer feed network.

Table 4. is presented as a comparison to several other 8×8 Butler matrix networks in the literature. Upon comparison, it can be noted that the integrated filters, and 1D/2D top layer arrays come at the expense of physical size and utilizing a non-inline design.

IV. FABRICATION AND MEASUREMENTS

The bottom-layer feed network and each of the top-layer arrays are fabricated separately. Nylon screws are used to fasten a selected array to the bottom-layer structure. Fig. 18 (a) depicts the fabricated system with the 1-D array attached; Fig. 18 (b) depicts the fabricated system with the 2-D array attached. The 1-D system is tested in the far-field anechoic chambers at the University of Victoria and Queens University, while the 2-D system is tested using the planar near-field scanner at the University of Waterloo’s CAIRS facility.

During simulation of the 1-D and 2-D structures, dielectric waveguide ports were used to feed the structures; to this end, lengthy computational time was significantly reduced. In order to approximate the measured results as closely as possible to the simulated results, TRL calibration standards are used to mitigate the effects of end-launch connectors and

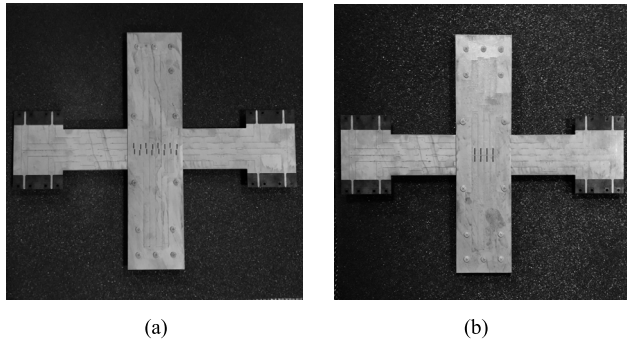


FIGURE 18. Beamforming network prototypes. 1-D array installed (left) and 2-D array installed (right).

TABLE 4. Comparison of several 8 × 8 Butler matrices in the literature.

	[20]	[23]	[22]	[10]	[13]	This Design
Freq (GHz)	3	22	2.44	60	29.5	30
Size (λ ²)	1.3x1	22x6.8	N/A	15x8	10x4	23.5x19.4
Technology	Stripline	Waveguide	Microstrip	SIW	SIW	SIW
Inline Design	No	Yes	No	Yes	Yes	No
Number of Cross-overs	6	16	0	16	8	8 and 6
Layers	1	1	1	1	2	2
Cascaded with Array(s)	No	No	Yes	Yes	Yes	Yes
1D/2D Expression	No	No	No	No	No	Yes
Integrated Filters	No	No	No	No	No	Yes

microstrip transitions that feed the realized structure. During testing, a single input port is excited while the remaining ports are terminated with microwave absorbent material. It should be noted, however, that during measurement of the beam patterns, reflections were observed in the outer most beams. In order to mitigate the effects of the reflections, the full structures around the arrays, the end-launch connectors, and the input cable connectors, were coated in microwave absorbing material. In this manner, the absorbent material was able to reduce reflections and scattering.

The simulated and measured reflection coefficients of ports 1 through 4 are presented in Fig. 19 (a) for the 1-dimensional beamforming network. Due to the staggered layout of the antenna array (Fig. 8), asymmetries arise in the reflection coefficients of ports 5 through 8 when compared to ports 1 through 4. These deviations are noted but considered minor, and for the purpose of this paper are considered symmetric. The measured return loss is observed to be better than 14.3 dB over the operating frequency range, and better than 23.4 dB at 30 GHz. The simulated and measured results for the isolation can be seen in Fig. 19 (b) and (c) for ports 1 and 2, respectively. The measured isolation is observed to be better than 11.5 dB over the operating frequency range. The return loss and isolation levels for the remaining ports are similar. Note that the isolation parameter S_{72} is higher than that of other paths (Fig. 19 (c)). This, in part, can be attributed to the layout of the array, as well as the top SIW layer cross-over couplers. This isolation parameter is

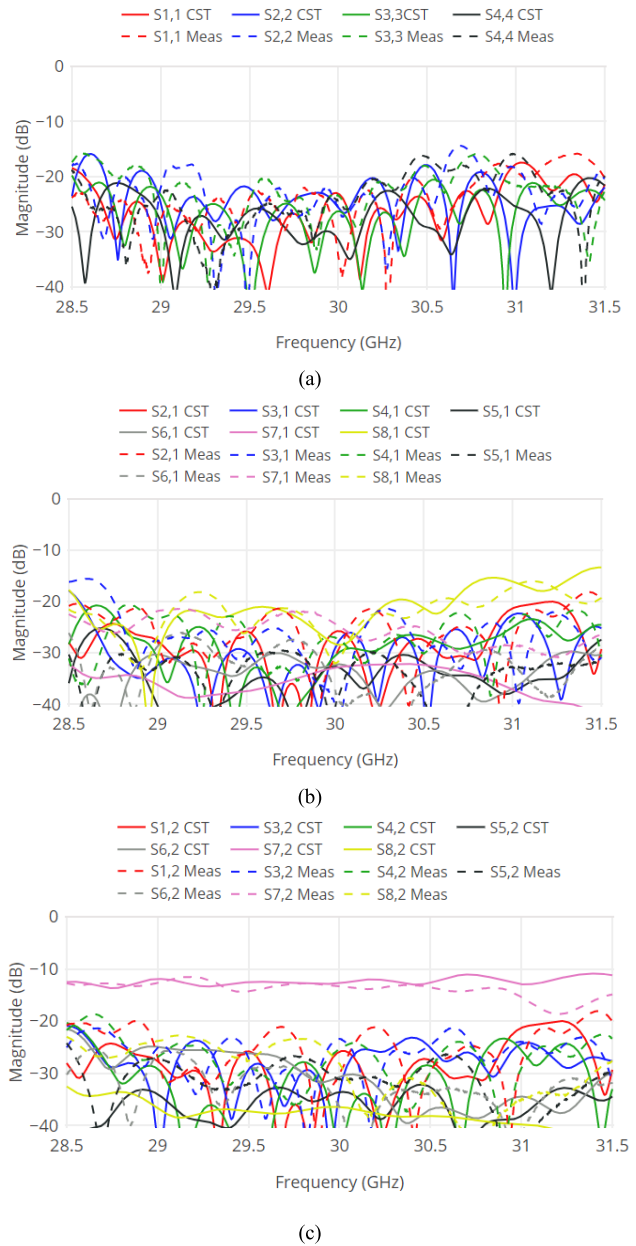


FIGURE 19. Simulated and measured reflection coefficients and isolation for the 1-D beamforming system.

shown to be improved in the 2-D system on the account of the alternative array layout, which in turn, does not require cross-over couplers in the top layer (Fig. 13).

Demonstrating the beam patterns at two representative frequencies, the normalized simulated and measured 1-D beam patterns are shown in Fig. 20 (a) and (b) for 29.5 GHz and 30.5 GHz, respectively. The gain of the antenna system is calculated for ports 1 through 4 at the specified points: 28.5 GHz, 29 GHz, 29.5 GHz, 30 GHz, 30.5 GHz, 31 GHz, and 31.5 GHz. Fig. 21 illustrates a measured gain of 7.6 dB to 13.0 dB for the 1-D array example.

The simulated and measured reflection coefficients of ports 1 through 4 are presented in Fig. 22 (a) for the 2-D beamforming network. The measured return loss is observed

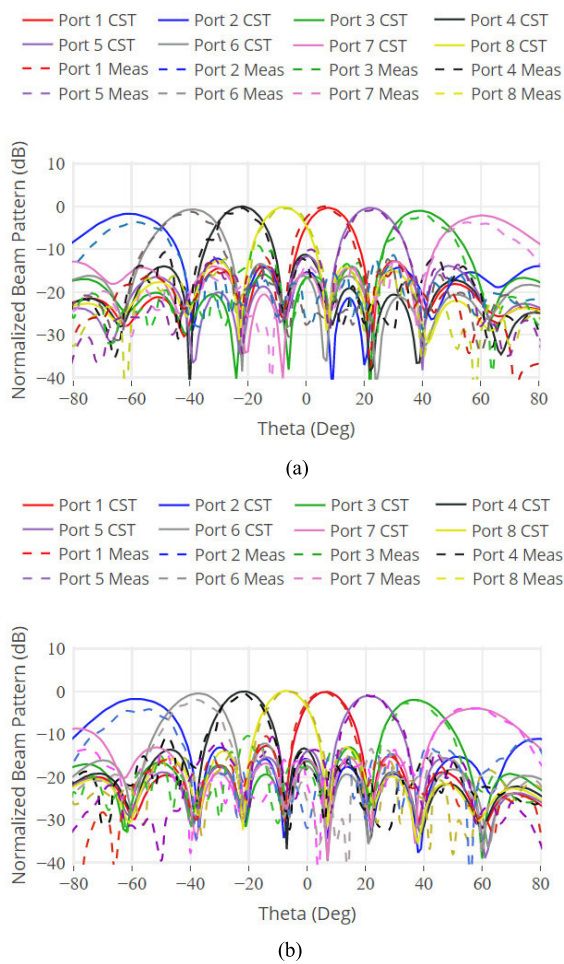


FIGURE 20. Normalized simulated and measured 1-D beam patterns at (a) 29.5 GHz, and (b) 30.5 GHz.

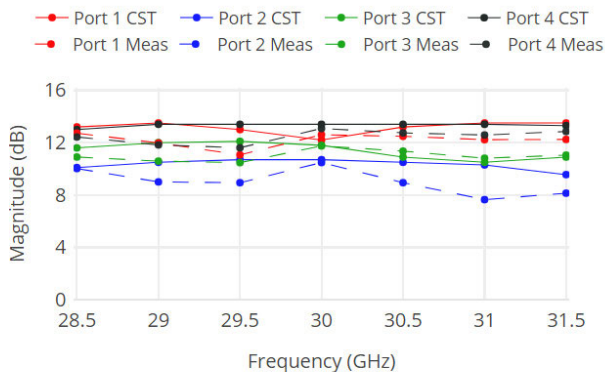


FIGURE 21. Simulated vs measured gain of ports 1 through 4 for the 1-D beamforming network.

to be better than 13.6 dB over the operating frequency range, and better than 17.6 dB at 30 GHz. The simulated and measured results for the isolation can be seen in Fig. 22 (b) and (c) for ports 1 and 2, respectively. The measured isolation in ports 1 and 2 are better than 13.8 dB. The return loss and isolation levels for the remaining ports are similar as well. Additionally, it can be noted that that isolation parameter S_{72}

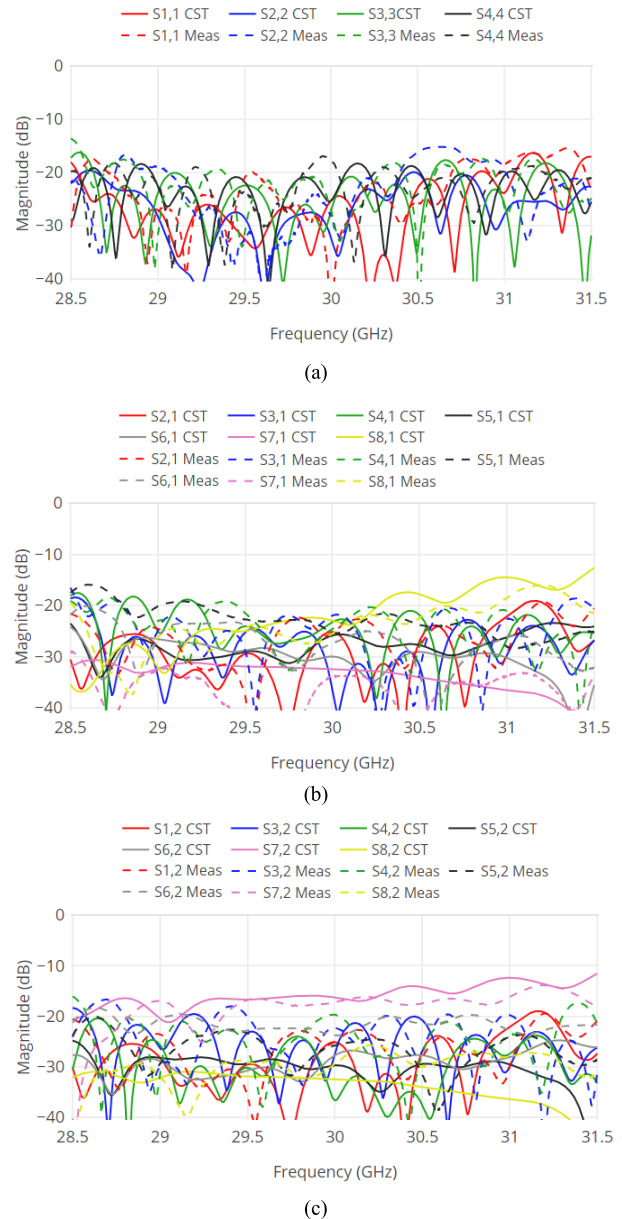


FIGURE 22. Simulated and measured reflection coefficients and isolations for the 2-D beamforming system.

in Fig. 22 (c) has been reduced significantly when compared to that of the 1-D system (Fig. 19 (c)).

Demonstrating the beam patterns at two representative frequencies, a comparison of the normalized simulated and measured 2-D beam patterns of ports 1 through 4 are shown in Fig. 23 (a) and (b) for 29.5 GHz and 30.5 GHz, respectively. The gain of the antenna system is calculated for ports 1 through 4 over the frequency range at the specified points: 29 GHz, 29.5 GHz, 30 GHz, 30.5 GHz, and 31 GHz. Fig. 24 illustrates a measured gain of 7.6 dB to 10.1 dB for the 2-D array example.

For both the 1-D and 2-D examples in this work, the measured results agree closely with the simulated results, thus validating the design approach and feasibility of

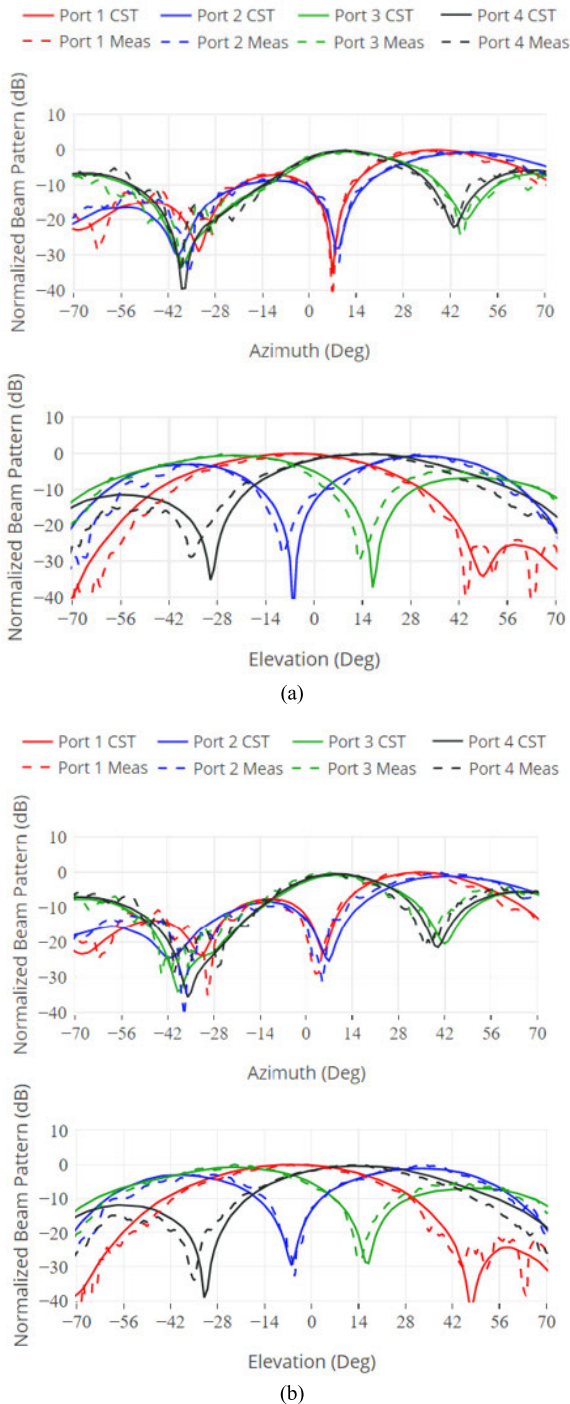


FIGURE 23. Normalized simulated and measured 2-D beam patterns at (a) 29.5 GHz, and (b) 30.5 GHz.

the 8×8 cross-configuration Butler matrix as a beamforming network in SIW technology. Physical reconfigurability of the system is an important attribute for future applications that may require different beam specifications; restrictions such as cost and the impact of environmental surroundings can be taken into account in this manner. The location of passband filters between the top and bottom SIW layers also allows for more versatile configurations that can include expanded array

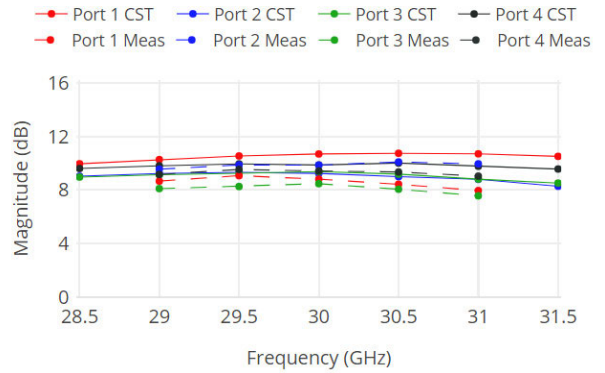


FIGURE 24. Simulated vs measured gain of ports 1 through 4 for the 2-D beamforming network.

sizes, as well as the integration of larger or more stringent filters to be designed.

V. CONCLUSION

An 8×8 SIW cross-configuration Butler matrix with interchangeable one-dimensional and two-dimensional slot antenna arrays is presented for operation between 28.5 and 31.5 GHz. The simulated and measured 10 dB bandwidth is demonstrated over a range of 28.5 to 31.5 GHz. The measured gain of the 1-D array system is 7.6 dB to 13.0 dB with a wide horizontal scanning range. At 30 GHz, the range is approximately $\pm 60.0^\circ$. The measured gain of the 2-D array system over 29 to 31 GHz is 7.6 dB to 10.1 dB with a 2-D scanning range. At 30 GHz, the horizontal scanning range is approximately $\pm 44.0^\circ$ and the vertical scanning range is approximately $\pm 32.0^\circ$. The presented results validate the design approach of the dual-layer beamforming network employing interchangeable top layer arrays. Although only two simple examples are illustrated, future work can explore more creative – or dramatic – beam patterns as well as utilize folded dual-layer filters with more application specific constraints such as the introduction of transmission zeros.

ACKNOWLEDGMENT

The authors greatly acknowledge Mr. Ian Goode and Dr. Carlos Saavedra of Queens University for their help and expertise with far-field measurements, as well as Dr. Aidin Taeb and Dr. Safieddin Safavi-Naeini of the CAIRS facility at the University of Waterloo for their help and expertise with near-field measurements.

REFERENCES

- [1] K. Wu, D. Deslandes, and Y. Cassivi, “The substrate integrated circuits—A new concept for high-frequency electronics and optoelectronics,” in *Proc. 6th Int. Conf. Telecommun. Modern Satell., Cable Broadcast. Service*, vol. 1, Oct. 2003, pp. 1–8.
- [2] D. Deslandes and K. Wu, “Accurate modeling, wave mechanisms, and design considerations of a substrate integrated waveguide,” *IEEE Trans. Microw. Theory Techn.*, vol. 54, no. 6, pp. 2516–2526, Jun. 2006.
- [3] M. Bozzi, A. Georgiadis, and K. Wu, “Review of substrate-integrated waveguide circuits and antennas,” *IET Microw. Antennas Propag.*, vol. 5, no. 8, pp. 909–920, Jun. 2011.

- [4] T. Djerafi, N. J. G. Fonseca, and K. Wu, "Design and implementation of a planar 4×4 Butler matrix in SIW technology for wideband applications," in *Proc. 40th Eur. Microw. Conf.*, Paris, France, Sep. 2010, pp. 910–913.
- [5] T. Djerafi and K. Wu, "Multilayered substrate integrated waveguide 4×4 Butler matrix," *Int. J. RF Microw. Comput.-Aided Eng.*, vol. 22, no. 3, pp. 336–344, Feb. 2012.
- [6] Q. Wu, J. Hirokawa, J. Yin, C. Yu, H. Wang, and W. Hong, "Millimeter-Wave multibeam endfire dual-circularly polarized antenna array for 5G wireless applications," *IEEE Trans. Antennas Propag.*, vol. 66, no. 9, pp. 4930–4935, Sep. 2018.
- [7] C. Bartlett, S. S. Hesari, and J. Bornemann, "End-fire substrate integrated waveguide beam-forming system for 5G applications," in *Proc. Int. Symp. Antenna Technol. Appl. Electromagn.*, Waterloo, ON, Canada, Aug. 2018, pp. 1–4.
- [8] N. Tiwari and T. R. Rao, "A switched beam antenna array with Butler matrix network using substrate integrated waveguide technology for 60 GHz wireless communications," *AEU-Int. J. Electron. Commun.*, vol. 70, no. 6, pp. 850–856, Jun. 2016.
- [9] T. Djerafi and K. Wu, "A low-cost wideband 77-GHz planar Butler matrix in SIW technology," *IEEE Trans. Antennas Propag.*, vol. 60, no. 10, pp. 4949–4954, Oct. 2012.
- [10] Y. Li and K.-M. Luk, "A multibeam end-fire magnetoelectric dipole antenna array for millimeter-wave applications," *IEEE Trans. Antennas Propag.*, vol. 64, no. 7, pp. 2894–2904, Jul. 2016.
- [11] X. Cheng, Y. Yao, T. Tomura, J. Hirokawa, T. Yu, J. Yu, and X. Chen, "A compact multi-beam end-fire circularly polarized septum antenna array for millimeter-wave applications," *IEEE Access*, vol. 6, pp. 62784–62792, Nov. 2018.
- [12] J.-W. Lian, Y.-L. Ban, Y.-Q. Wu, and L.-H. Zhong, "Compact 28-GHz two-dimensionally scanning multibeam array with sidelobe suppression," in *IEEE MTT-S Int. Microw. Symp. Dig.*, Chengdu, China, May 2018, pp. 1–4.
- [13] L.-H. Zhong, Y.-L. Ban, J.-W. Lian, Q.-L. Yang, J. Guo, and Z.-F. Yu, "Miniaturized SIW multibeam antenna array fed by dual-layer 8×8 Butler matrix," *IEEE Antennas Wireless Propag. Lett.*, vol. 16, pp. 3018–3021, 2017.
- [14] Q.-L. Yang, Y.-L. Ban, J.-W. Lian, Z.-F. Yu, and B. Wu, "SIW Butler matrix with modified hybrid coupler for slot antenna array," *IEEE Access*, vol. 4, pp. 9561–9569, 2016.
- [15] Q.-L. Yang, Y.-L. Ban, K. Kang, C.-Y.-D. Sim, and G. Wu, "SIW multibeam array for 5G mobile devices," *IEEE Access*, vol. 4, pp. 2788–2796, 2016.
- [16] Y. J. Cheng, W. Hong, and K. Wu, "Millimeter-wave multibeam antenna based on eight-port hybrid," *IEEE Microw. Wireless Compon. Lett.*, vol. 19, no. 4, pp. 212–214, Apr. 2009.
- [17] Y. J. Cheng, K. Wu, and W. Hong, "Substrate integrated waveguide (SIW) broadband compensating phase shifter," in *IEEE MTT-S Int. Microw. Symp. Dig.*, Boston, MA, USA, Jun. 2009, pp. 845–848.
- [18] Z. Kordiboroujeni and J. Bornemann, "Designing the width of substrate integrated waveguide structures," *IEEE Microw. Wireless Compon. Lett.*, vol. 23, no. 10, pp. 518–520, Oct. 2013.
- [19] J. Butler and R. Lowe, "Beam-forming matrix simplifies design of electronically scanned antennas," *Electron. Des.*, vol. 9, pp. 170–173, Apr. 1961.
- [20] K. Wincza, S. Gruszczynski, and K. Sachse, "Broadband planar fully integrated 8×8 Butler matrix using coupled-line directional couplers," *IEEE Trans. Microw. Theory Techn.*, vol. 59, no. 10, pp. 2441–2446, Oct. 2011.
- [21] K. Wincza and S. Gruszczynski, "Broadband integrated 8×8 Butler matrix utilizing quadrature couplers and Schiffman phase shifters for multibeam antennas with broadside beam," *IEEE Trans. Microw. Theory Techn.*, vol. 64, no. 8, pp. 2596–2604, Aug. 2016.
- [22] G. Adamidis and I. Vardiambasis, "Smart antenna design and implementation: A simple switched-beam antenna array based on a 8×8 Butler-matrix network," in *Proc. 10th WSEAS Int. Conf. Commun.*, Athens, Greece, Jul. 2006, pp. 473–478.
- [23] S. Yamamoto, J. Hirokawa, and M. Ando, "A single-layer hollow-waveguide 8-way Butler matrix," in *IEEE AP-S Int. Symp. Dig.*, Washington, DC, USA, Jul. 2005, pp. 647–650.



CHAD BARTLETT was born in Nelson, BC, Canada, in 1987. He received the B.Eng. degree in electrical engineering from the University of Victoria, in 2017, where he is currently pursuing the master's degree. His primary research interests include microwave and millimeter-wave passive component design, Butler matrices, and filter component design.



JENS BORNE MANN (M'87–SM'90–F'02) received the Dipl.Ing. and Dr.Ing. degrees in electrical engineering from the University of Bremen, Germany, in 1980 and 1984, respectively.

From 1984 to 1985, he was an Engineering Consultant. In 1985, he joined the University of Bremen, Germany, as an Assistant Professor. Since April 1988, he has been with the Department of Electrical and Computer Engineering, University of Victoria, Victoria, BC, Canada, where he became a Professor, in 1992. From 1992 to 1995, he was a Fellow of the British Columbia Advanced Systems Institute. In 1996, he was a Visiting Scientist with Spar Aerospace Limited (now MDA Space), Ste-Anne-de-Bellevue, QC, Canada, and a Visiting Professor with the Microwave Department, University of Ulm, Germany. From 1997 to 2002, he was the Co-Director of the Center for Advanced Materials and Related Technology (CAMTEC), University of Victoria. In 2003, he was a Visiting Professor with the Laboratory for Electromagnetic Fields and Microwave Electronics, ETH Zürich, Switzerland. He has coauthored *Waveguide Components for Antenna Feed Systems-Theory and Design* (Artech House, 1993) and has authored/coauthored more than 350 technical articles. His research interests include RF/wireless/ microwave/millimeter-wave components and systems design, and field-theory-based modeling of integrated circuits, feed networks and antennas. He is also a Fellow of the Canadian Academy of Engineering (CAE) and the Engineering Institute of Canada (EIC). From 1999 to 2009, he has served on the Technical Program Committee of the IEEE MTT-S International Microwave Symposium. From 1999 to 2002, he has served as an Associate Editor for the IEEE TRANSACTIONS ON MICROWAVE THEORY AND TECHNIQUES in the area of Microwave Modeling and CAD. From 2006 to 2008, he was an Associate Editor of the *International Journal of Electronics and Communications*. He serves on the Editorial Advisory Board for the *International Journal of Numerical Modeling*. He is also a Registered Professional Engineer in the Province of British Columbia, Canada.

• • •